Prediction of Hydrofracture of Rock Salt under Ground at the Waste Isolation Pilot Plant

지하 핵 폐기물 저장 암염의 파괴현상 검증 및 분석

Heo, Gwang－Hee*1
허 광 희
Lee, Cheo－Keun*2
이 처 근
Heo, Yol*3
허 열

요 지

WIPP에서 가스로 인한 파괴의 가능성을 해석적 계산과 수치해석 및 실내실험을 통하여 연구하였다. 우선 본 연구와 관련된 화학반응식을 조사한 결과, 폐기물 내의 철이 산화하면서 다량의 가스가 발생될 수 있음을 알았다. 또한 간단한 지하수 흐름의 계산결과, 투수성이 높은 파쇄영역이 존재하지 않는 경우 이 가스량은 암염 내부와 약한 수평면에 인장균열을 초래하기에 충분히 높은 압력을 야기시킬 것이다. 해석적 계산은 선형탄성파괴역학의 개념을 사용하여 수행하였고, 수치해석은 유한요소법을 사용하여 행하였다. 또한 실내실험은 발생가능한 파괴 메카니즘을 설명하기 위하여 행하였다. 해석결과 약한 경석고층에서 수평으로 균열이 증가된 뒤에 그 균열은 이 층을 뚫고나가 암염 위쪽으로 계속 전파되어 지표면 쪽의 수평방향과 53° 경사각을 갖고 지표면에 도달된다. 이와 같은 후자의 현상을 방지하기 위하여 경석고는 암염의 인성보다 0.5590배가 적은 파괴인성을 가져야 하는 것으로 나타났다. 실험결과 세 가지 형태의 균열(radial vertical cracks, horizontal circular cracks and cone－shaped cracks)이 관찰되었다.

Abstract

The possibility of the development of gas－driven hydrofractures at the Waste Isolation Pilot Plant(WIPP) is investigated through analytical and numerical calculations and through laboratory experiments. First, an investigation of the chemical reactions involved shows that a large volume of gas could potentially be generated through the oxidation of iron in the waste. Simple ground water flow calculations then show that unless regions of high permeability has been created, this gas volume will build up the pressure high enough

*1 University of New Mexico 토목공학과 박사과정 수료

*2 정회원 · 충북대학교 대학원 토목공학과 박사과정 수료

*3 정회원 · 충북대학교 공과대학 토목공학과 교수

to cause tensile damage in the horizontal planes of weakness or in the halite itself. The analytical calculations were performed using the concepts of linear elastic fracture mechanics and the numerical calculations were done using the finite element method. Also, laboratory tests were conducted to illustrate possible failure mechanisms. It is possible that after growing horizontal crack in the weaker anhydrite layer, the crack could break out of this layer and propagate upward into the halite and toward the ground surface at an inclined angle of around 53° above horizontal. To prevent this latter phenomenon, the anhydrite must have a fracture toughness less than 0.5590 times than that of the halite. Through the tests, three types of crack(radial vertical cracks, horizontal circular cracks and cone-shaped cracks) were observed.

1. Introduction

All of the calculations in this research assume, unless otherwise stated, the following gas generation model :

The number of models, n, of gas generated is assumed to be given by :

$$\begin{aligned} &n=(2\text{mole/year drum})\times(6800\text{ drums/room})\times(120\text{ rooms}) \text{ for } 0<t<550\text{ years}\\ &n=(1\text{mole/year drum})\times(6800\text{ drums/room})\times(120\text{ rooms}) \text{ for } 550<t<1050\text{ years}\\ &n=(0\text{mole/year drum})\times(6800\text{ drums/room})\times(120\text{ rooms}) \text{ for } 1050\text{ year}<t \end{aligned} \quad (1)$$

To check the reasonableness of this number for total potential mass of gas, assume that an average barrel of waste contains, say, 50kg of iron or 895 moles of iron. Consider the following set of chemical reactons :

$$\begin{aligned} &Fe^0 = Fe^{2+} + 2e\\ &2H^+ + 2e^- = H_{2(g)}\\ &\overline{Fe^0_{(s)} + 2H^+ = Fe^{2+} + H_{2(g)}} \end{aligned} \quad (2)$$

(one molecule of gaseous H_2)

$$\begin{aligned} &2(Fe^{2+} = Fe^{3+} + e^-)\\ &2H^+ + 2e^- = H_{2(g)}\\ &\overline{2Fe^{2+} + 2H^+ = 2Fe^{3+} + H_{2(g)}} \end{aligned} \quad (3)$$

(one molecule of gaseous H_2)

$$\overline{Fe^{3+} + H_2O = F(OH)_{3(s)} = 3H^+} \quad (Fe(OH)_{3(s)}\ \textit{is rust}) \quad (4)$$

This reaction is enhanced when in the presence of brine. It can be seen that for every two iron atoms that rusts, three H_2 molecules of gas are greated. This means that $895\times 3/2=1343$ moles of H_2 gas are generated per drum, which accounts for most of the potential 1600 moles of H_2 per drum generated by the model above. The rate of this reaction as well as its equilibrium is not considered here.

A second general assumption is that the ideal gas law holds :

$$PV = nRT \tag{5}$$

where P is the gas pressure, V is the gas volume, n is the number of moles of gas, R is the ideal gas constant, and T is the absolute temperature.

The total volume of all the drum is (6800 drums / room) × (120 rooms) × (0.208m^3 / drum) = 169,728m^3. However, as the waste is initially rapidly compacted by the room closure due to creep, the drum will be compacted, and so an initial volume of waste and gas is somewhat uncertain, but would be some fraction of 169,728m^3. It is assumed in this research that the original volume of gas contained within the WIPP is 45,000m^3 at one atmosphere (0.1 MPa), or 304m^3 at 14.8 MPa. The potential volume of gas to be generated at a pressure of 14.8 MPa is 217,806m^3. It is thus seen that the number of moles of air originally in the room is negligible compared with the number of moles of that gas could potentially be generated. The rooms will probably creep to a minimum volume at about 150 years : it would therefore be reasonable to expect that almost all of the generated waste gas must be accommodated through room re-expansion, pore water displacement, borehole leak-off, gas-driven hydrofracture, or some other, as yet unidentified, mechanism.

The geometry of WIPP, for the purpose of this research, is approximated as being axisymmetric with respect to a vertical axis going through the center of the repository[1]. The depth of the repository is assumed to be 659m below the ground surface. Horizontal Markerbed 139 is assumed to be hydraulically connected to the repository, and at the same elevation (even though it is actually several meters below the floor of the repository). The repository is assumed to be a thin horizontal penny-shaped crack, 500m in radius.

2. Flow prior to rock damage

Before proceeding any further with predictions of damage to the rock (halite or anhydrite), it is necessary to understand what is the resisting behavior of flow in the undamaged halite or anhydrite layers. The permeabilities of rock salt and anhydrite 10^{-22} m^2, and 10^{-19}m^2, respectively[9].

Assume that two types of flow are possible : radial outward flow through the anhydrite of Markerbed 139, and vertical flow upward to the top of the Salado, 300m above the repository. The ambient pore pressure in the anhydrite is assumed to be 9.0 MPa, while that at the top of the Salado is assumed to be 5MPa[10].

Darcy's law is given by

$$v_s = -\frac{k}{\mu}\left(\frac{dH}{ds}\right) \tag{6}$$

where v_s is the velocity of fluid flow in direction s. k is the intrinsic permeability of the rock and μ is the viscosity of brine. k and μ are assumed constant in this calculation, as the rock is assumed to be undamaged. The variable H is the hydraulic head, equal to the pressure p minus the hydrostatic pressure ρgh.

2.1 Estimate of radial flow into the anhydrite

First, consider radial flow of the brine in Markerbed 139. For now, we neglect to consider storativity through compressibility of the brine. At any radial distance, r, from the center of the WIPP,

$$Q_H = 2\pi r b v_H = 2\pi r \frac{k}{\mu}\left(\frac{dH}{dr}\right) = \text{constant (incompressible flow)} \tag{7}$$

where b is the average thickness of the makerbed, and v_H is the velocity of radial flow. It follows that.

$$Q_H = \frac{2\pi b k}{\mu}(p_2 - p_1)\frac{1}{ln(r_2/r_1)} \tag{8}$$

evaluating, we get

$$Q_H = \frac{2\pi(1m)(10^{-18}m^2)}{0.0009\frac{kg}{sec \cdot m}}(14.8\times10^6 - 9.0\times10^6\frac{N}{m^2})\frac{1}{\ln(\frac{600m}{500m})} = 1.63\times10^{-8}\frac{m^3}{sec}$$

This is equivalent to 514m^3 per 1000 years. Obviously, the amount of fluid leaving the repository radially(to accomodate gas storage) is negligible compared to the amount of gas that needs to be accommodated(217,806m^3).

2.2 Estimate of vertical flow into the halite.

A similar calculation indicates that vertical flow, Q_v, of brine through the halite also produces negligible gas storage volume :

$$v_v = \frac{k}{\mu}\left(\frac{dH}{ds}\right) \cong \frac{k}{\mu}\left(\frac{\Delta H}{\Delta s}\right) \tag{9}$$

where H=pressure head=$p-\rho gh$, v_v is the velocity of vertical flow, and s is the elevation.

Therefore

$$Q_v = v_v A = \frac{k}{\mu}\left(\frac{\Delta H}{\Delta s}\right)\pi(r_1)^2 \tag{10}$$

$$Q_v = \frac{10^{-22} m^2}{0.0009 \frac{kg}{sec \cdot m}} \left(\frac{[(14.8-6.46)-(5.0-3.52)] \frac{10^6 N}{m^2}}{300m} \right) \pi (500m)^2 = 2.0 \times 10^{-9} \frac{m^3}{sec}$$

Thus the total vertical flow upward from the repository, prior to damage in the halite, but after the gas pressure reaches lithostatic pressure, is $63m^3$ per thousand years. Again, this is not nearly the amount of flow needed to keep the gas pressure below lithostatic pressure.

2.3 Estimate of storativity in anhydrite

Now let us determine whether the storativity of brine due to its compressibility is important or not. The compressibility of water, E_v, is equal to the pressure, p divided by the volumetric strain, ε_v :

$$p = E_v \varepsilon_v \tag{11}$$

The compressibility of water is 2.07×10^9 N/m^2. The total volume of water contained within Markerbed 139, assumed 1m thick, within a radius of 6000m, assuming 2.7% porosity, is approximately $3 \times 10^6 m^3$. Thus, if this total volume of water is compressed from 9 MPa to 14.8 MPa, its volume decreases by

$$\Delta V = \frac{\Delta p}{E_v} V = \frac{(9.0-14.8) \times 10^6 \frac{N}{m^2}}{2.07 \times 10^9 \frac{N}{m^2}} 3.0 \times 10^6 m^3 = -8406 m^3 \tag{12}$$

The decreased volume of water is an order of magnitude and it is too small to accommodate the expected amount of generated gas.

The bulk modulus of halite and anhydrite(approximately 31,000MPa) is an order of magnitude higher than the bulk modulus of the water(approximately 2,070MPa), and therefore, at least under elastic deformations, little storativity due to pore expansion would be expected.

3. Application of damage caused by pore pressure in geomaterials.

Now let us apply the concepts of fracture mechanics and damage mechanics to the gas-driven hydrofracture problem at WIPP. For simplicity, assume that the halite(say, at a location 1000 meters from the repository and at the same elevation as the repository) is initially in a state of high hydrostatic confinement, with no deviatoric stresses. Such is known to be the case for the undisturbed halite, which has over time crept like a fluid un-

til all, or at least most, of the deviatoric stresses are eliminated. (If the matrix were allowed to creep until all deviatoric stresses were eliminated, then the pore pressure within the matrix would necessarily be equal to the overburden pressure. If this is the case, then there would be no pressure gradient driving fluid from the repository until the gas pressure exceeded the lithostatic pressure, at which point tensile damage would commence. It would be interesting to measure the pore pressure in truly undisturbed halite, as this information could be used to determine if halite has a threshold deviatoric stress below which creep stops. it is unclear how this measurement could best be made.)

Thus, the effective state of stress on the matrix is $p_e = p_o - p_p$, where p_e is the effective pressure on the rock matrix, p_o is the total overburden stress, and p_p is the pore pressure, assumed hydrostatic. Assuming some slight degree of volumetrically distributed hydraulically connected porosity as the pore pressure is increased to equal the lithostatic pressure, p_o, the effective pressure on the rock matrix drops to zero. One big question is : Is the permeability a function of effective compressive hydrostatic stress? And if so, what is that function?

As the pore pressure is increased further, the effective stress on the rock matrix becomes tensile, causing tensile damage within the matrix. Usually, once significant tensile damage begins to occur, the stress of rock is close to its tensile strength, σ^*, as shown in Fig. 1. An important question is how much damage, D^*, has occurred when the stress of rock is at its tensile strength? After the tensile stress of the rock has been reached to its tensile strength, the stress begins to decrease with increasing strain, as indicated in by the descending branch of the stress−strain curve shown in Fig. 1.

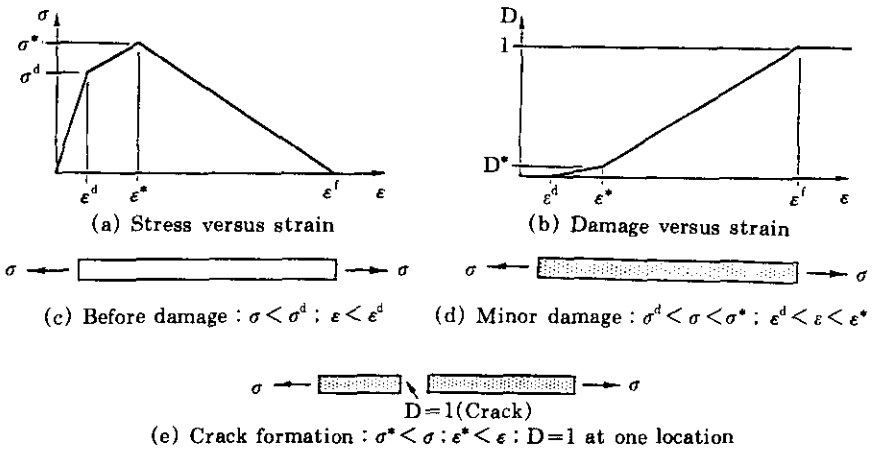

Fig.1 The formation of damage in a uniaxial tension specimen.

At the tensile stress, σ^d, where damage becomes evident, localization of this damage is imminent. The reason for this is that regions of the highest tensile damage will have

higher subsequent rates of damage because the effective tensile hydrostatic stress is higher there. Thus, the meaning of the descending branch in Fig. 1 is open to question, because as soon as the tensile stress of the rock is reached to its strength, a "strain localization" occurs, leading to very large tensile strains over very short lengths, that is to say, a crack. Thus, it makes more physical sense to represent the descending portion of the stress−strain curve shown in Fig. 1 as a stress versus crack opening displacement (COD) curve, as shown in Fig.2.

A well accepted model for tensile damage in geomaterials is the cohesive crack model[7]. The cohesive crack model assumes that minimal damage, D, occurs until the tensile stress of the rock is reached to its strength, after which a localized post−peak damage occurs under decreasing tensile traction, as shown(using simplified linear functions) in Fig.2.

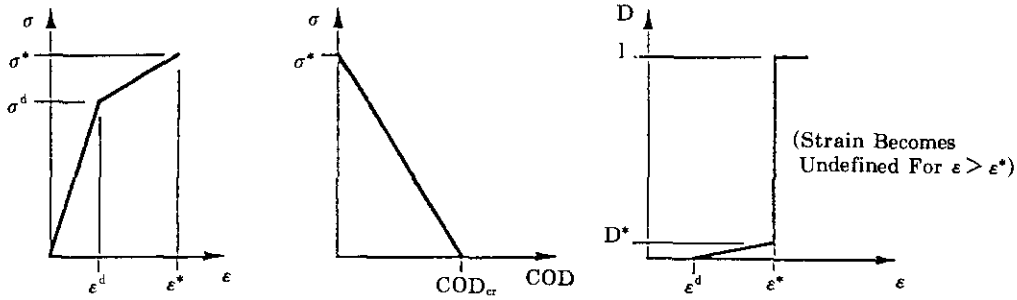

(a) Stress versus tensile strain (b) Stress versus COD (c) Damage versus tensile strain

Fig.2 The cohesive crack model

A consequence of the assumption that damage occurs mainly under conditions of decreasing tensile traction is that the damage will tend to localize to a single surface, rather than to multiple surfaces. Fig.3 shows schematically why this is the case. A way to think about tensile damgne is to consider the material as a chain composed of individual links. As the chain is stretched to failure, only the weakest link will break, leading immediately to unloading of all of the other links.

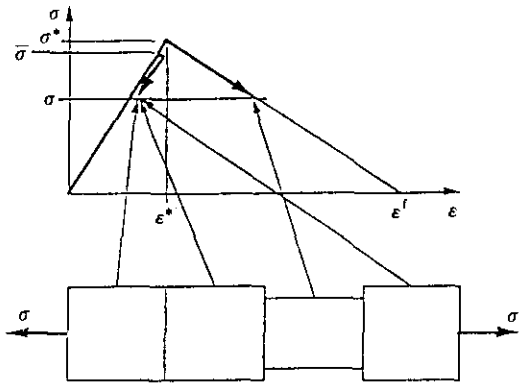

Fig.3 Why strain localization occurs in strain −softening materials

The idea of microcrack coalescence to a single macrocrack due to pore pressure is caused by an initial damage leads to increased permeability and it leads to increased pore pressure. This pore pressure leads to increased damage and it leads to increased permeability. This positive feedback loop results in what is often called "material instability" due to tensile strain softening.

An example of this type of behavior is the development of damage in a toy balloon. It would be wrong to argue that in this case of a rubber balloon, that damage forms as a volumetric distribution of simultaneously growing microcracks. In a balloon, as soon as one "microcrack" dominates in size, it will grow much more rapidly than its smaller neighbors, leading to failure of the balloon.

In conclusion, it appears that if damage occurs in salt due to tensile effective stress caused by large pore pressures, this damage is likely to manifest itself almost immediately as a discrete crack, rather than as a cloud of volumetrically distributed and hydraulically connected microcracks. This leads to the next chapter, which considers the propagation of a gas-driven hydrofracture in the anhydrite, which is considered as the "weak link" in the chain.

4. Calculations of hydrofracture in anhydrite

4.1 The theory of LEFM

The theory of LEFM, developed over the course of this century[3, 5, 6] has as its basis the notions that (1) except for the fracture process zone(FPZ) close to the crack tip within which inelastic material behavior occurs, the material within the crack propagates follows Hooke's law; and (2) the size of the FPZ is small compared to other dimensions in the problem.

Assumption (2) that the FPZ is small compared to other dimension in the problem seem to be valid because we are discussing crack lengths here on the order of kilometers in length, and all indications are that in salt and anhydrite the FPZ length is not more than, and probably much less than, a meter in length. We therefore proceed with the assumption that LEFM will give a reasonable prediction of cracking behavior under the conditions in which it is applied in this study. We caution, however, that other cracking situations at WIPP probably require fracture models more sophisticated than LEFM.

4.2 Calculations for short crack

It can be approximated as a penny shaped crack in an infinite medium, subjected to internal pressure and remote applied overburden stress, as shown in Fig. 4(a). This approximation is valuable because an exact theoretical stress-intensity factor solution

exists. We make the assumption here that the geometry of the storage rooms can be neglected, with little effect upon the stress-intensity factor solution. The stress intensity factors K_I and K_{II} and crack opening displacement, Δ, are given, according to as[8] :

$$K_I = \frac{2}{\pi}(P-\sigma_o)\sqrt{\pi \bar{a}} \; ; \; K_{II} = 0 \tag{13}$$

$$\Delta = \frac{8(1-\nu^2)}{\pi E}(P-\sigma_0)\sqrt{\bar{a}^2-\gamma^2} \tag{14}$$

where P is the gas pressure, σ_0 is the overburden stress $\bar{a}$ is the crack length, ν is the Poisson's ratio, and E is the Young's modulus.

Now assume that under conditions of crack propagation the pressure, p, in the system is equal to the pressure that causes crack growth, P_{crit}, and under this condition $K_I = K_{IC}$. Rewriting Eq.(13), we obtain :

$$P_{crit} = \frac{K_{IC}}{2}\sqrt{\frac{\pi}{\bar{a}}} + \sigma_0 \tag{15}$$

The volume of the crack, V_{crack}, is determined by integrating the crack opening displacement, Δ, over the surface area of the crack :

$$V_{crack} = \frac{16(1-\nu^2)(P_{crit}-\sigma_0)\bar{a}^3}{3E} \tag{16}$$

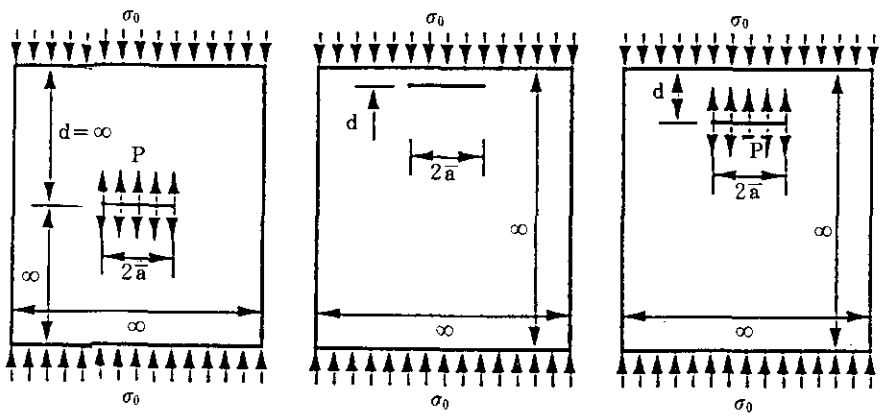

(a) Short crack($\bar{a}$ /d~0) (b) Long crack($\bar{a}$/d~∞) (c) Medium crack($\bar{a}$/d~1)

Fig.4 Modeling assumptions(Note that d=659m is constant in calculations)

We assume that the halite and the anhydrite layer have no available volume for gas storage during crack propagation

$$P_{crit}(V_{room} + V_{crack}) = nRT \tag{17}$$

The number of models of gas generated is assumed to be given by Eq. (1). Nonlinear equations (15), (16), and (17) can and have been solved numerically for the unknown variables P_{crit}, V_{cracks}, and $\bar{a}$ as a function of time. Solutions for crack length, $\bar{a}$, volume, V, over pressure, $(P-\sigma_0)$, and maximum crack opening displacement, Δ_{max}, for serveral different input parameters are shown in Fig. 5.

4.3 Calculations for long crack

There is another bounding case for which it is possible to obtain exact stress-intensity factors and crack opening displacement : the case in which the circular crack is very long compared to its depth of embedment in an elastic half space. In this case, the material above the crack can be considered to be a thin circular elastic plate, clamped at its boundary at the radius of the crack front. The material below the crack can be considered to be infinitely stiff compared to the stiffness of the plate above the crack. This solution would be expected to be very accurate for crack with radius more than about ten times their embedment depth.

The out-of-plane displacement, w, for a circular plate, clamped at its boundary and loaded laterally with a uniform pressure, p, is given by :

$$w = \frac{p}{64D}(\bar{a}^2 - r^2)^2, \text{ where the plate modulus is given by} \tag{18}$$

$$D = \frac{Ed^3}{12(1-\nu^2)} \tag{19}$$

By integrating the displacement, w, times the applied traction, p, over the area of the plane, we obtain the potential energy, Π, in the problem :

$$\Pi = \frac{1}{2}\int_{r=0}^{r=\bar{a}}\int_{\theta=0}^{\theta=2\pi} pw(r\,d\theta)dr = \frac{\pi p^2 \bar{a}^6}{384D} \tag{20}$$

Now, the energy release rate, G, can be obtained as

$$G = \frac{\partial \Pi}{\partial A} = \frac{\partial \Pi}{\partial \bar{a}}\frac{\partial \bar{a}}{\partial A} = \frac{\pi p^2 \bar{a}^4}{128D} \tag{21}$$

Recognizing that $(K_I)^2 = \frac{EG_I}{(1-\nu^2)}$, $(K_{II})^2 = \frac{EG_{II}}{(1-\nu^2)}$, we obtain the following stress-in-

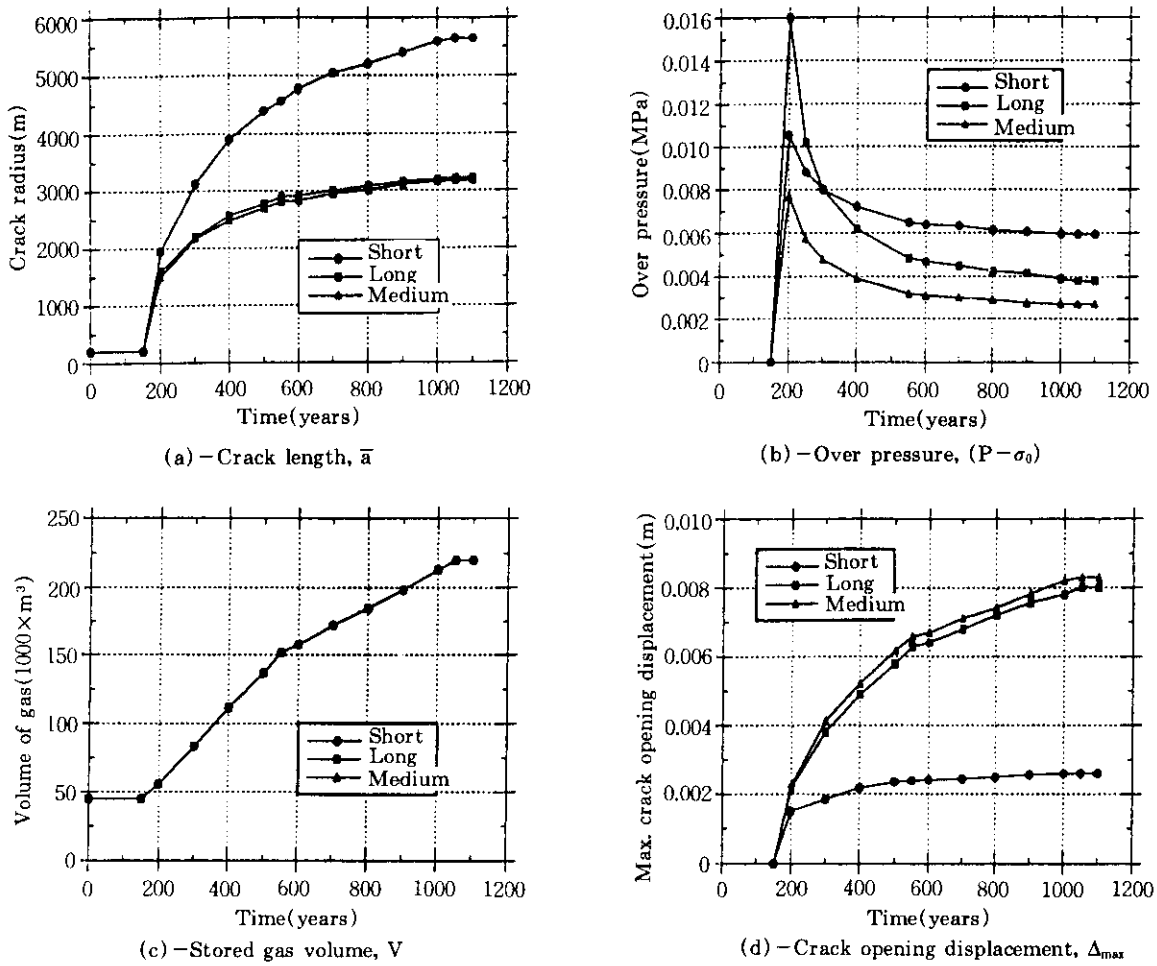

Fig. 5 Various responses vs. time for horizontal, circular, gas−driven hydrofracture, for short, medium, and long crack models.

tensity factor solution :

$$K_I = K_{II} = \frac{\sqrt{3}p\bar{a}^2}{8d\sqrt{d}} \tag{22}$$

The volume, V_{crack} enclosed by the crack is found by integrating the crack opening displacement, $\Delta=w$, over the area of the plate to obtain :

$$V_{crack} = \frac{\pi p\bar{a}^6}{192D} = \frac{\pi p\bar{a}^6(1-\nu^2)}{16Ed^3} \tag{23}$$

Now, by substituting these new expressions for K_I and V_{crack} into Eqs. (16)~(18) above,

and solving these three equations numerically, we obtain the results shown in Fig.5.

4.4 Calculations for medium crack

As can be seen from Fig.5(a), we are predicting a horizontal crack with ultimate radius on order of 2 km$<r<$6 km($3<\bar{a}/d<9$). Unfortunately, neither the "long crack" nor the "short crack" solution is valid for this range of $\bar{a}/d$ ratios. Because we know of no published solutions for this intermediate case, we resorted to finite element calculations to obtain approximate solutions for K_{I}, K_{II} and Δ. We performed finite element calculations for horizontal axisymmetric cracks, subjected to internal pressure, p, of lengths 500m, 1000m, 2000m, 3000m, 4000m, 5000m, and 6000m, all at d=659m embedment depth. Stress intensity factors were extracted from quarter-point quadratic crack tip elements using the displacement correlation method[4]. Two deformed meshes are shown in Fig. 6 : one for a short crack and the other for a long crack. The shapes of the crack opening profiles for the short and the long crack are in sharp contrast.

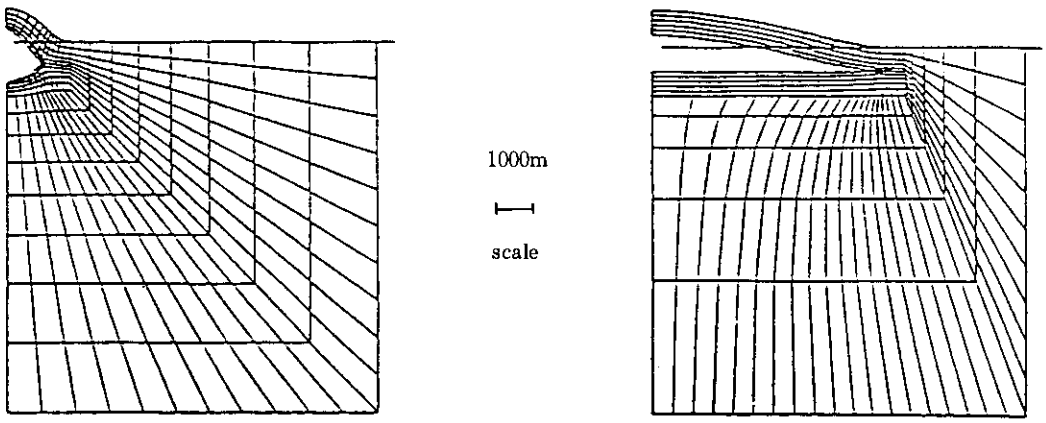

(a) Close-up of crack area(Crack length $\bar{a}=1000$m)　　(b) Entire mesh(Crack length $\bar{a}=6000$m)

Fig.6 Deformed meshes(deformations greatly magnified) for "short" and "long cracks.

By using a curve-fitting approach to the data and also by ensuring that the approximating functions asymptotically approach the "short crack" and the "long crack" solutions, we developed the following approximate formulas for K_{I}, K_{II}, and Δ_{max} as function of $\bar{a}/d$:

$$K_{\text{I}} = p\sqrt{\bar{a}}\left[\frac{2}{\sqrt{\pi}} - 0.1125\sqrt{\frac{\bar{a}}{d}} + 0.03505\frac{\bar{a}}{d} + \frac{\sqrt{3}}{8}\left(\frac{\bar{a}}{d}\right)^{3/2}\right] \tag{24}$$

$$K_{\text{II}} = p\sqrt{\bar{a}}\left[0.08903\sqrt{\frac{\bar{a}}{d}} - 0.1827\frac{\bar{a}}{d} + \frac{\sqrt{3}}{8}\left(\frac{\bar{a}}{d}\right)^{3/2}\right] \tag{25}$$

$$\Delta_{max} = \frac{p\bar{a}(1-\nu^2)}{E}\left[\frac{8}{\pi} + 0.3890\frac{\bar{a}}{d} + 0.3159\left(\frac{\bar{a}}{2}\right)^2 + \frac{3}{16}\left(\frac{\bar{a}}{d}\right)^3\right] \tag{26}$$

The volume, for the intermediate case, assuming that the crack profile is as in the long crack case, is approximated by :

$$V_{crack} = \frac{\pi \Delta_{max} \bar{a}^2}{3} \tag{27}$$

Again, by substituting these new expressions for K_I and V_{crack} into Eqs. (16)~(18) above, and solving these three equations numerically, we obtain the results shown in Fig. 5.

5. Mixed-mode hydrofracture in Rock Salt

5.1 K_I and K_{II} for a horizontal circular crack near a free surface

5.1.1 Internal crack pressure loading

We have been unable to find any published stress-intensity factor solutions for a horizontal circular crack near a free surface subject to internal pressure, P. We have considered the limiting case of a small crack compared to its depth of embedment. In such a case, by symmetry considerations, there can be no Mode II component of stress-intensity factor. We have also been able to calculate the exact energy release rate, G, for a crack that is very large compared to its distance frome the free surface by considering it as a circular plate clamped at its outer edge. However, we have been unable to analytically decompose this solution into Mode I and Mode II components. Therefor we have resorted to numerical method to obtain approximate ratios of K_{II} to K_I.

Fig.7 shows the results of finite element calculations, in which we have calculated, normalized K_I and K_{II} results as a function of normalized crack length, $\bar{a}/d$. It appears from the figure that K_{II} approaches K_I as the crack radius becomes large compared to its depth. It is unknown whether K_{II} exactly approaches K_I as the crack becomes very large compared to its depth, but we assume that is the case. Further work is required to determine this limiting ratio definitively.

5.1.2 Gravitational body forces acting on surrounding medium

Gravitational body forces acting upon the surrounding medium will tend to close the crack, causing negative K_I and a K_{II} opposite in sign to that caused by internal pressurization. Again, no published solution have been found for such a case, so we must resort to analytical and numerical methods.

Consider first a short crack. The stress field in the medium is assumed to be increasing hydrostatically with depth (since the salt has crept to relieve shear stresses over the eons). If a horizontal crack were introduced, it would clearly tend to close, causing a negative $K_I = -\sigma_0(\bar{a})^{1/2}$. K_{II}, on the other hand, is related only to the crack length, $\bar{a}$, and the density of the material, but is unaffected by the overburden pressure, σ_0. Therefore K_{II}

would be negligible compared to K_I.

Next consider a long crack. The deformation field of the material on top of the crack would be essentially the same, but opposite to that of the pressurized crack discussed in the last section.(The material on top of the plate approaches a uniformly loaded clamped plate ; the material below approaches a no−crack deformation condition.) The sign of K_{II} would tend to cause the crack to propagate in a downward direction, assuming the crack side could overlap, which of course, they can't.

For a medium crack, finite element calculations are required to determine the stress−intensity factors. We have not performed a detailed analysis of this case, although this certainly could be done. Instead, as a discussed in Section 5.3, we have considered the case of a crack simultaneously loaded with body forces and internal pressurization.

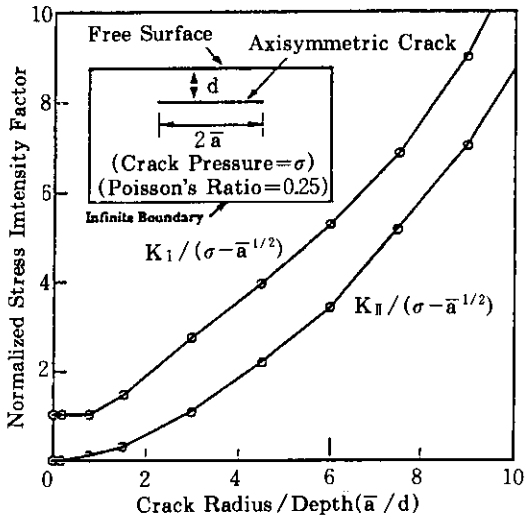

Fig.7 Stress intensity factors for pressurized embedded horizontal circular crack near a free surface, calculated using the finite element method.

5.2 Conditions for the crack to propagate out of the weak layer

As the crack length to depth ratio ($\bar{a}$ /d) becomes larger, the Mode II stress−intensity factor, K_{II}, grows until for very long cracks, ($\bar{a}$ /d=infinity) it is apparently equal to K_I. Thus mixed−mode, curvilinear cracking is a possibility. The tendency is for the crack to tend to "dish" upward as it propagates. However, because the anhydrite layer is expected to be less tough than the halite above it, there is also a tendency for the crack to continue to propagate within the weaker anhydrite layer. By using a mixed−mode theory of crack progagation, we can determine the ratio of $K_{Ic(salt)}$ to $K_{Ic(anhydrite)}$ necessary to prevent the crack from deviating from the anhydrite layer.

For simplicity, we choose the maximum circumferential tensile stress criterion for

mixed-mode crack propagation[2]. This theory says that the crack will propagate perpendicular to the direction of maximum circumferential tensile stress, $\sigma_{\theta max}$, if $\sigma_{\theta max}$ reaches a critical material constant value. Mathematically, the theory is stated as

$$\sigma_\theta\sqrt{2\pi r} = constant = \cos\frac{\theta_0}{2}\left(K_I \cos^2\frac{\theta_0}{2} - \frac{3}{2} K_{II} \sin\theta_0\right) = K_{Ic} \tag{28}$$

where the angle, θ_0, (perpendicular to which is the maximum circumferential tensile stress) is given by the parametric equation.

$$K_I \sin\theta_0 + K_{II}(3\cos\theta_0 - 1) = 0 \tag{29}$$

Now, considering the case of a long crack, we asswume that $K_I = K_{II}$. Therefore, we can solve Eq. (29) for θ_0 ; we obtain $\theta_0 = 53°$ above horizontal. For the case where $\theta_0 = 53°$, we must assume that $K_{Ic}/K_{Ic(salt)}$. For this case, from Eq. (29), we find that the crack will propagate into the salt if $K_I > 0.5590 K_{Ic(salt)}$.

The other possiblity is that the crack will progagate in the plane of the anhydrite layer. In this case, we insert $\theta_0 = 0°$ and $K_{Ic} = K_{Ic(anhydrite)}$ into Eq. (29). In this case, we find that the crack will propagate horizontally if $K_I > K_{I(anhydrite)}$.

Now, which path will the crack that? If $K_{Ic(anhydrite)} < 0.5590 K_{Ic(salt)}$, the crack will propagate horizontally, within the anhydrite layer. On the other hand, if $K_{Ic(anhydrite)} > 0.5590 K_{Ic(salt)}$, the crack will begin to propagate upward into the salt at an angle of 53°. The ratio of fracture toughness of salt to that of anhydrite is thus a crucial parameter in determining the behavior of the crack.

5.3 Trajectory of a pressurized circular crack near a free surface with body forces

We have run into an unexpected and interesting problem when attempting to perform mixed-mode crack propagation analyses of a pressurized crack with body forces included. We find that the direction of crack propagation is extremely sensitive to small errors in the calculated stress-intensity factors. To explain the problem, we must explain our algorithm in more detail.

Our algorithm for gas driven hydrofracture makes use of two independent sets of stress-intensity factors : those due to gravitational body forces (K_I^B, K_{II}^B), and those due to a pressure of unit magnitude (K_I^P, K_{II}^P). The stress-intensity factors at the crack tip are the superposition of these independently calculated ones :

$$K_I = K_I^B + PK_I^P \tag{30}$$

$$K_{II} = K_{II}^B + PK_{II}^P \tag{31}$$

These two equations can then be inserted into Eqs. (28) and (29), and solved for P and θ. We find, however, that although P is insensitive, θ is extremely sensitive to K_{II}^{B} and to K_{II}^{P}. Because both of these numbers are an order of magnitude lower than K_{I}^{B} and K_{I}^{P}, small errors in their calculation seem to make big differences in θ.

For the crack to propagate, it seems that K_I should be positive, yet our calculations show that the crack can grow with slightly negative K_I, because of the still-significant K_{II}(compared to K_{Ic}), causing the crack to dip downward. If we assume that K_I must be equal to K_{Ic} for the crack to propagate, K_{II} changes in sign, and the crack is predicted to grow upwards. So we find that the direction of crack growth depends strongly upon our assumptions and upon the accuracy with which the Mode II stress-intensity factors are calculated.

Fig. 8 shows the failure envelope predicted by the maximum circumferential tensile strength criterion plotted on the K_I-K_{II} plane. This envelope shows that crack propagation can occur even if K_I is negative, as long as there is sufficient K_{II}. However, we have strong reason to believe that the effective fracture toughness rapidly increases as K_I becomes negative, because of frictional drag between the crack sides. As a method to recify the dilemma, we could increase K_{Ic} by several orders of magnitude of above the usually accepted Mode I fracture toughness for the material. The justification for increasing the fracture toughness is that if indeed the crack were to propagate while K_I was still negative, there would be large frictional forces between the crack faces(the crack would not yet be open), and thus a large amount of energy would be dissipated. Using this assumption, and assuming that $K_{Ic}=1500$ MPa$(m)^{1/2}$, we were able to predict the results shown in Fig. 9.

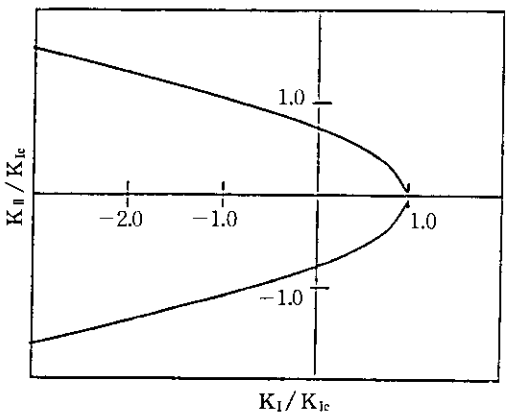

Fig.8 Failure envelope predicted by maximum circumferential tensile stress criterion.

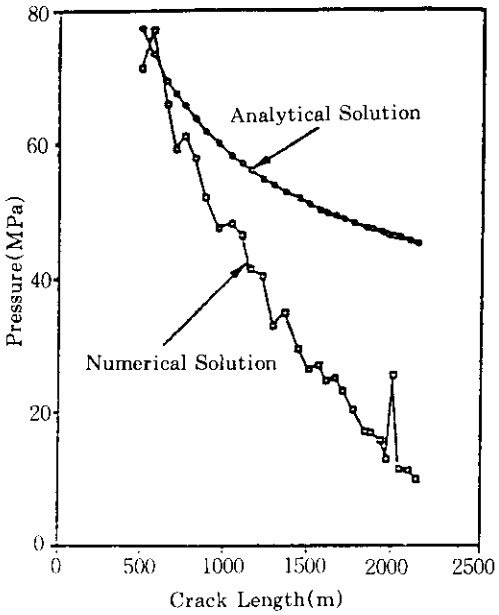

(a) Pressure vs. crack length

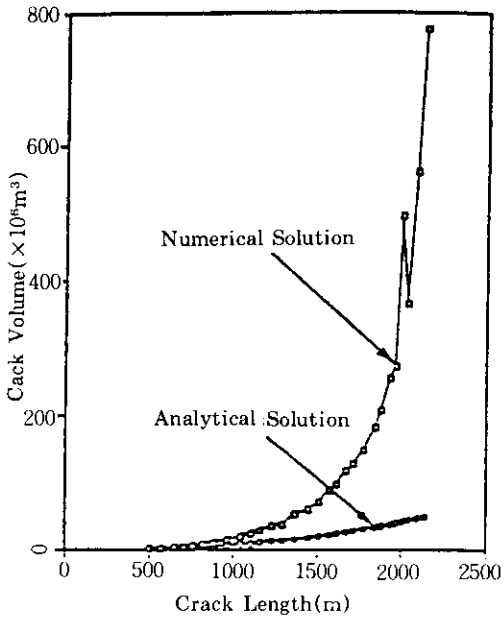

(b) Volume vs. crack length

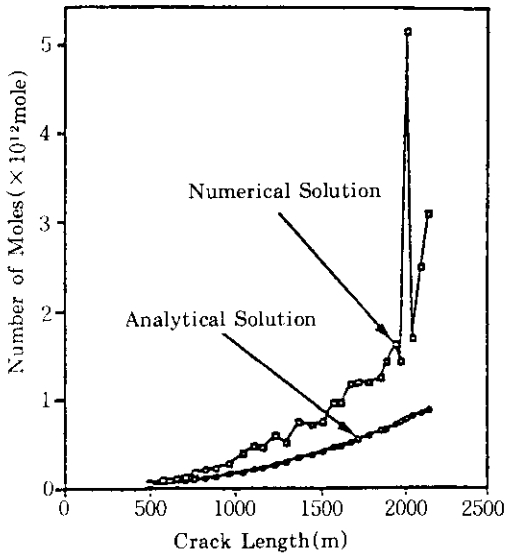

(c) Mass of gas vs. crack length

Fig.9 Graphs of equilibrium pressure, crack volume, and number of moles of gas as a function of crack length(With gravitational loading)

6. Laboratory modeling of hydrofracture at WIPP

The main objectives of this laboratory tests were to determine if our calculations are

meaningful, or if we are missing the point altogether as a scoping exercise to determine what types of crack were possible. So, we assumed it is a reasonable laboratory modeling to see the following questions :

(1) Is it appropriate to use the assumptions of linear elastic fracture mechanics (LEFM) to predict gas-driven hydrofracture?

(2) Is dynamic fracture a possibility?

(3) Are multiple cracks possible?

The models consisted of two layers of transparent acrylic glued together, as shown in Fig.10, supported, to simulate the stiffness of the ground beneath the Salado, by an almost rigid box. The top layer was 3/8″ thick, and the bottom layer was 3/4″ thick. A storage room was simulated by machining a circular, penny-shaped cavity, 1/8″ deep, and of diameter varying from 1/2″ to 2″, in the top of the bottom layer of acrylic. The acrylic layers were glued together with glue (WELD-ON 4(a strong glue), WELD-ON 35 (a

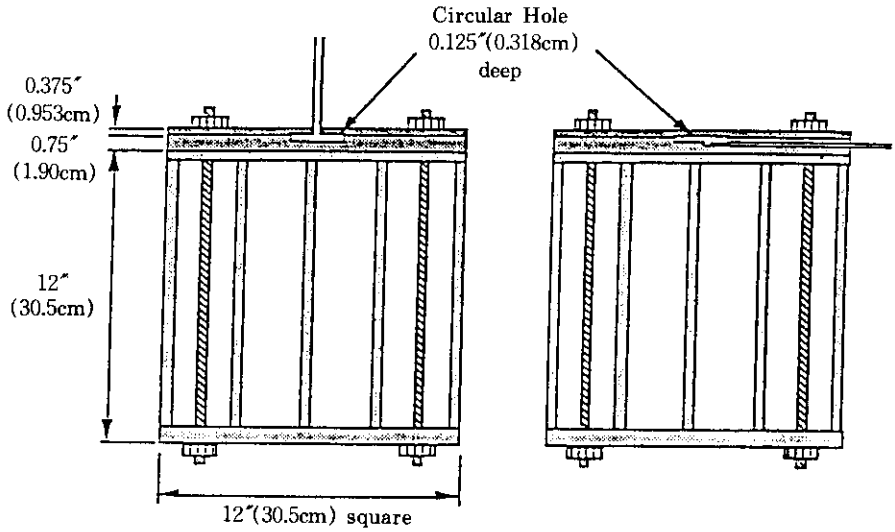

(a) Top entry model (b) Side-entry model

Fig.10 Sketch of test arrangements

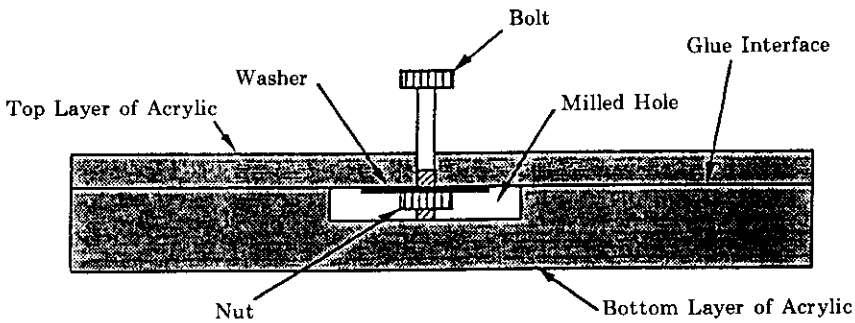

Fig.11 Sketch of wedge-opening bolt and nut arrangement

weak glue), or water (a very weak glue)), to simulate the layers of anhydrite within the salt layers. It was possible to simulate non homogeneous anhydrite layers by using glues of varying strength. A 1/4″ diameter hole was bored, through which colored liquid and/or air was pumped into the penny-shaped storage room to simulate the build-up of waste gases.

To get a "feel for the material", the initial stresses (1 and 2) were performed with a bolt that applied a wedge-opening load, as shown in Fig. 11. These tests showed that the WELD-ON 35 was weaker than the acrylic layers, so that a situation in which the crack was confined to the weaker layer was obtained. On the other hand, the WELD-ON 4 was sufficiently strong that cracking that took place tended to be in the acrylic, rather than in the glue joint.

In test 3 through 6 a 1/4″ threaded vertical hole concentric with the penny-shaped cavity, as shown in Fig. 10(a), was used to introduce pressurized fluid to the model. Because we found that this threaded hole and associated fitting seemed to affect the cracking behavior, the subsequent tests were performed with a horizontal hole, as shown in Fig. 10 (b).

Test 6 through 17 were performed using green-dyed water as the hydrofracturing fluid. Water was used, rather than air, because we wanted to avoid extremely dynamic failures. In tests 18 and 19, air was used to simulate more closely the situation at WIPP. In test 20, water was used, rather than glue, to determine whether water has sufficient surface tension to act, essentially, as a glue.

We also used LEFM to predict the pressures at which cracking was expected to commence, and compared these pressures to the experimental data in Fig. 12. In predicting failure pressure, we assumed that K_{Ic} was equal to 1.1 MPa(m)$^{1/2}$, and used the LEFM equation (15).

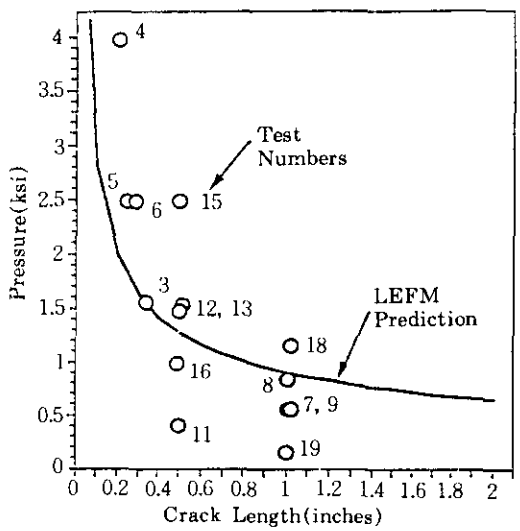

Fig. 12 Comparison of LEFM predictions of failure pressure with experimental results.

7. Conclusions

From this study on the prediction of gas-driven hydrofractures about rock salt under ground at the Waste Isolation Pilot Plant through analytical and numerical calculations and through laboratory experiments, the following conclusions can be drawn :

1. If a gas-driven hydrofracture develops in the anhydrite layer of Markerbed 139, it is predicted to develop rapidly about 150 years after the WIPP is sealed, as shown in Fig. 5(a). Over the next thousand years it will grow slowly to a final radius of approximately 3000m, as shown in Fig. 5(a). The pressure in the crack as it is growing will remain just slightly above the lithostatic pressure of 14.8 MPa, as shown in Fig. 5(b). The maximum crack opening displacement, at the center of the circular crack, will be approximately 8mm in width, as shown in Fig. 5(d).
2. Short cracks relative to their depth tend to propagate horizontally, whereas longer cracks tend to propagate upward due to internal crack pressurization.
3. If $K_{\mathrm{I\,c(anhydrite)}} < 0.5590\ K_{\mathrm{I\,c(salt)}}$, the crack will propagate horizontally, within the anhydrite layer. On the other hand, if $K_{\mathrm{I\,c(anhydrite)}} > 0.5590\ K_{\mathrm{I\,c(salt)}}$, the crack will begin to propagate upward into the salt at an angle of 53°. With body forces included, the crack trajectory at WIPP is extremely sensitive to the crack propagation theory and to small errors in the Mode II stress-intensity factors, $K_{\mathrm{II}}^{\mathrm{B}}$ and to $K_{\mathrm{II}}^{\mathrm{P}}$. By increasing the fracture toughness in such a case by a factor of 100, we were still able to get results.
4. Through the tests, three general types of cracking were observed : radial vertical cracks in the top layer(when using the top-entry model), horizontal circular cracks confined between the layers(when using the weaker WELD-ON 35 glue) and cone-shaped cracks propagating from the cavity to the top of the top layer (when using the strong WELD-ON 4 glue). The observed trends matched the LEFM predictions remarkably well. Also, comparison of the analytical and numerical LEFM predictions with the crack trajectories observed are as expected. We conclude that LEFM, although not perfect for predicting the behavior of the tests, is certainly a very reasonable approximation. The fact that failure pressure is generally a decreasing function of crack length, as shown in Fig. 12, indicates that dynamic fracture is a strong possibility, expecially when gas is used as the hydrofracturing fluid.

References

1. Arguello, J. G, and C.M. Stone.(1994), Internal Memorandum, to F.T. Mendenhall, Div. 6345, Sandia National Laboratories, Albuquerque, New Mexico.
2. Erdogan, F. and G.C. Sih. (1963), "On the Crack Extension in Plates Under Plane Loading and Transverse Shear", ASME Journal of the Basic Engineering, Vol.85, pp.519~527.
3. Griffith, A.A.(1920), "The Phenomenon of Rupture and Flow in Solids", Philosophical Transactions, Royal Society of London, Series A, V.221, pp.163~198.
4. Ingraffea, A.R. and V. Saouma. (1985), "Numerical Modeling of Discrete Crack Propagation in

Reinforced and Plain Concrete", Fracture Mechanics of Concrete, Sih., G. C. and DiTommaso, A., Eds., Martinus Nijhoff, pp. 171~225.

5. Irwin, G.R.(1957), "Analysis of Stresses and Strains Near the End of a Crack Traversing a Plate", ASME J. Applied Mechanics, Vol.24, pp.361~364.
6. Kreig, R.D.(1984), "Reference Stratigraphy and Rock Properties for the Waste Isolation Pilot Plant(WIPP) Project", SAND 83~1908, Sandia National Laboratories, Sandia National Laboratories, Albuquerque, New Mexico.
7. Mendenhall, F.T. and W.H.Gerstle.(1993), "WIPP Anhydrite Fracture Modeling", Internal Memoeandum, to Distribution, Sandia National Laboratories, Albuquerque, New Mexico.
8. Tada, H.,P.C. Paris, and G.R.Irwin.(1985), "The Stress Analysis of Cracks Handbook", Del Research Corp., Hellertown, Pennsylvania.
9. Stoelzel, D.,P.Vaughn, J.Bean, and J. Schreiber.(1994), 1994 Performance of Untreated Wastes for the Undisturbed Repository : Comparison to 1992 PA, Preliminary Results & Sampled Consequences vs. Mean / Median Calculation, Sandia National Laboratories, Albuquerque, New Mexico.
10. Wawersik, W.R., and C.M. Stone.(1998), "A Characterization of Pressure Records in Inelastic Rock Demonstrated by Hydraulic Fracturing Measurements in Salt", International Journal of Rock Mechanics and Mining Sciences and Geomechanics Abstracts, Vol.26, No.6, 613~627.

(접수일자 1995. 5. 24)